Spontaneous formation of Mn nanocluster arrays on a Si(111)-7×7 surface observed with STM

Jun-Zhong Wang,[1,2] Jin-Feng Jia,[3,2] Zu-Hong Xiong,[1] and Qi-Kun Xue[3,2,*]

[1]*School of Physics Science and Technology, and MOE Key Laboratory on Luminescence and Real-Time Analysis, Southwest University, Chongqing 400715, People's Republic of China*

[2]*State Key Laboratory for Surface Physics, Institute of Physics, Chinese Academy of Sciences, Beijing 100080, People's Republic of China*

[3]*Department of Physics, Tsinghua University, Beijing 100084, People's Republic of China*

(Received 4 March 2008; revised manuscript received 14 May 2008; published 22 July 2008)

An extreme low-deposition rate has been used to fabricate highly ordered Mn nanocluster arrays on A Si(111)-7×7 surface. Scanning tunneling microscopy (STM) studies reveal that the Mn nanoclusters prefer to occupy the faulted half-unit cells of the Si(1110)-7×7 with preference fraction ~95%. High-resolution STM images demonstrate that two types of three-dimensional Mn nanoclusters coexist in the arrays; one is an identical triangle cluster and the other is an off-center pear cluster. A planar identical Mn cluster has been obtained at the initial deposition stages, indicating the coverage-dependent Mn clustering. Careful analysis of the initial adsorption stage of Mn reveals that individual Mn atoms prefer to occupy the bridging B_2 sites around Si rest atoms and the substitution site of Si center adatoms. The formation mechanism of Mn nanocluster arrays is attributed to the delicate balance between thermodynamic tendency and kinetic limitation.

DOI: 10.1103/PhysRevB.78.045424 PACS number(s): 68.37.Ef, 68.65.Hb, 68.43.Hn

I. INTRODUCTION

There have been intensive studies on the fabrication of ordered metal nanocluster arrays stimulated by the novel physical and chemical properties arising from quantum-size effect. Significant progress in atomic engineering makes it possible to build highly-ordered nanostructures on suitable substrates today by self-organization techniques. Several approaches have been used to fabricate the self-assembled nanoclusters by taking advantage of suitable templates, such as the Si(111)-7×7 surface,[1–3] the reconstructed Au(111) surface,[4] and the strain-relief patterns of Pt(111).[5] In particular, the highly corrugated Si(111)-7×7 surface has been shown to be very suitable for the fabrication of perfect nanocluster arrays of group-III metals[6,7] through fine regulation of deposition rate and substrate temperature. For most metals, the structural difference between neighboring half-unit cells (HUCs) of Si(111)-7×7 would give rise to two inequivalent occupation probabilities. Similar preferred occupation of other systems, such as Ag, Au, and Li, has also been reported.[8–10] Therefore, it might be a general route to fabricate metal nanocluster arrays on Si(111)-7×7 through tuning the dynamics of diffusing adsorbates and the preferred occupation of the faulted half-unit cells (FHUCs), only if the meta/Si interface is not reactive.

Very recently, growing attention has been focused on the magnetic nanoclusters of 3*d* transition metal because of the great potential in high-density magnetic storage and spintronics.[11] From the viewpoint of application, it will be highly desirable to fabricate magnetic nanostructures directly on the most common semiconductor Si substrate, following the procedure of group-III nanoclusters on Si(111)-7×7 template. However, for transition metals, this template seems unfeasible due to the strong interdiffusion and possible reactions between the magnetic adsorbate and substrate Si, the resultant silicides are unsuitable for spintronics. We realize that manganese, the unique transition-metal element, does not react with Si substrates at room temperature (RT) and may form nanostructures without silicide formation.[12]

There have been many reported studies on the Mn/Si(111) system, including the deposition of Mn films[13–17] and Mn nanoclusters fabrication[18–23] on Si(111)-7×7. RT depositions with post annealing result in the formation of large irregular clusters and small pyramidal and ring clusters,[20] but this procedure did not provide the periodic arrangement of the Mn clusters arrays. Following the procedure of group-III metal nanocluster,[2] ordered Mn nanocluster arrays have been reported on Si(111)-7×7 surface, utilizing elevated substrate temperature and low-deposition rate, which varied from 0.05 ML/min (Ref. 23) to 0.17 ML/min.[21,22] However, neither the local structures and symmetry of Mn clusters nor the occupation sites of individual Mn atoms have been obtained. Furthermore, the reported elevated substrate temperature between 180 °C to 260 °C might lead to the Mn/Si reaction.

According to the results from kinetic Monte Carlo simulation,[24] the optimal temperature window of metal clustering on Si(111)-7×7, corresponding to the crossover between the kinetic and thermodynamically controlled regimes, is higher than RT. To realize the preferred occupation of faulted HUCs, elevated substrate temperature is necessary. On the other hand, elevated substrate temperature is harmful to Mn/Si systems. One may ask if there is an alternate way to regulate the kinetics instead of using high-substrate temperature. It is known from growth dynamics that low-deposition rates produce similar effects as high-substrate temperatures. At low-deposition rate, the deposited adatoms are able to jump several times before another adatom landing, and the preference aggregation to the faulted HUCs are induced by the diffusion mechanisms. Therefore, this provides us a new way to regulate the growth kinetic for the unique Mn/Si system. To reduce the deposition rate low enough while keeping the substrate temperature near the same level, RT can produce the same effect of high-substrate temperature without the risk of Mn/Si reaction.

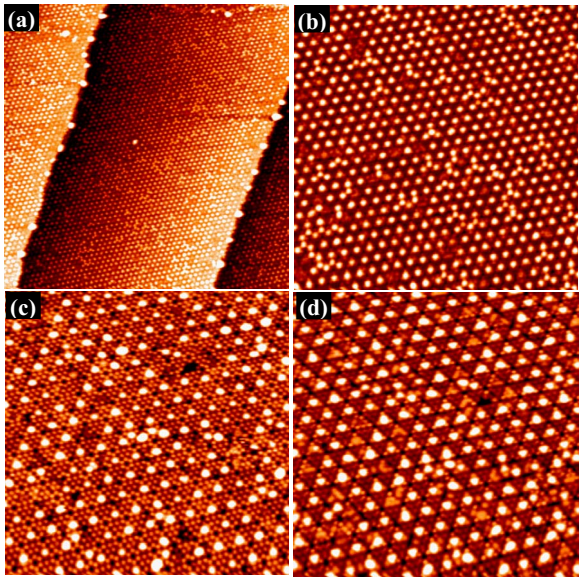

FIG. 1. (Color online) STM images of Mn nanocluster arrays formed on Si(111)-7×7 with ~0.18 ML Mn deposited at substrate temperature of 80 °C. (a) 145×145 nm^2, $U=-2.5$ V. (b) 60×60 nm^2, $U=-2.5$ V. (c) 35×35 nm^2, $U=+1.2$ V. (d) 35×35 nm^2, $U=-2.0$ V.

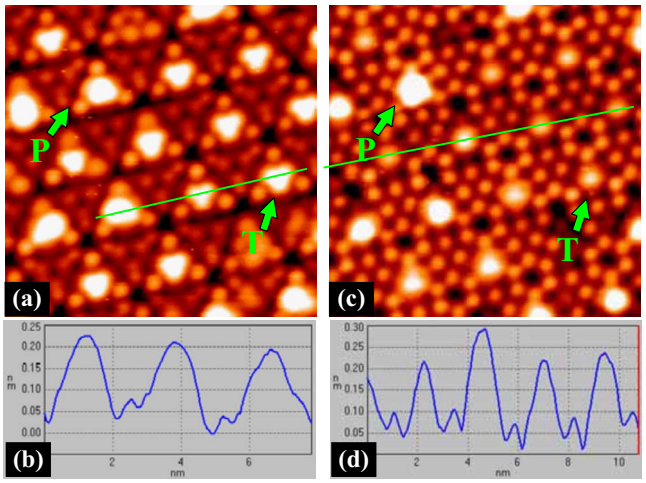

FIG. 2. (Color online) High-resolution STM images of the Mn nanoclusters. (a) Filled-state image, $U=-1.2$ V, 12×12 nm^2. (b) The cross-sectional line profile of the Mn nanoclusters along the solid line in Fig. 2(a). (c) Empty-state image, $U=+1.6$ V, 12×12 nm^2. (d) The cross-sectional line profile of the Mn nanoclusters along the solid line in Fig. 2(b). The clusters marked by *P* correspond to pear clusters and those marked by *T* correspond to the identical triangle clusters.

In this paper, an extreme low-deposition rate (~0.01 ML/min) has been used to deposit Mn on the Si(111)-7×7 surface with substrate temperature of ~80 °C. Highly-ordered Mn nanocluster arrays have been achieved. The fraction of preferred occupation of the faulted HUCs amounts to ~95%. Scanning tunneling microscopy (STM) observation reveals the coexistence of 3D identical triangular clusters and the pear clusters. The favored occupation sites of individual Mn atoms have been identified. Furthermore, studies on the initial deposition stage indicate that Mn clustering is a coverage-dependent process.

II. EXPERIMENTS

The experiments were performed with an Omicron variable-temperature STM operated in an ultrahigh vacuum 8×10^{-11} mbar. Clean Si(111)-7×7 surface was prepared by repeated resistive flashing procedures. A boron nitride crucible was used to produce Mn (purity 99.999%) atomic beams. The typical deposition rate is around 0.01 ML/min (1 ML=7.83×10^{14} Mn atoms/cm^2). The Mn flux was calibrated by the reconstruction of Si(111)-$\sqrt{3}\times\sqrt{3}$-Mn, where it takes at least 4 ML of Mn for the Si(111) surface to be entirely covered by $\sqrt{3}\times\sqrt{3}$ phase after annealing at 350 °C (Ref. 13). All STM images were recorded at RT in the constant current mode.

III. RESULTS AND DISCUSSION

Utilizing the extreme low-deposition rate around 0.01 ML/min, we fabricated the highly-ordered Mn nanocluster arrays on Si(111)-7×7 by depositing 0.18 ML Mn at substrate temperature 80 °C. Figure 1(a) shows the large-scale STM image for the morphology Mn nanocluster arrays, where periodic arrangement of the Mn nanoclusters with long-range ordering can be observed. Some irregular Mn islands appeared nearby the Si(111) steps. The cluster distribution becomes more evident from the middle-scale images shown in Fig. 1(b). The Mn clusters predominantly reside in the faulted HUCs of Si(111)-7×7 with the preference fraction around 95%, which is nearly the same as that of Tl on Si(111) (Ref. 1) and is higher than the reported Mn preference of 91%, optimized with a higher deposition rate.[21] This demonstrates the effect of utilizing an extremely low-deposition rate. Meanwhile, the "bright triangle stars" that appeared in Fig. 1(a) become clear that they are made of four neighboring clusters from three faulted HUCs and one unfaulted HUC. The cluster morphologies change significantly upon the polarity of sample bias changes. We noticed that in the empty-state image of Fig. 1(c), most of the Mn clusters exhibit a round appearance with a uniform size distribution. In the filled-state image shown in Fig. 1(d), the Mn clusters exhibit either a triangle or a pear shape. Most importantly, it is evident that all the triangle clusters have the identical appearance. Moreover, we find that the reconstruction of Si(111)-7×7 substrate remains intact after the cluster formation, indicating that no chemical reaction occurred between Mn and Si.

More structural information about the Mn nanoclusters can be obtained from the high-resolution STM images. From the filled-state image in Fig. 2(a), it is found that the identical triangle clusters, as marked by "*T*," are centered with HUCs, keeping the threefold symmetry of Si(111) substrate. Within the HUCs, three Si corner adatoms remain intact. Careful observation reveals that the triangle cluster edges have some extent of bending inwards, similar to the reported alkali clusters on Si(111)-7×7 (Ref. 25). In the empty-state image of Fig. 2(c), the identical triangle clusters exhibit a pronounced

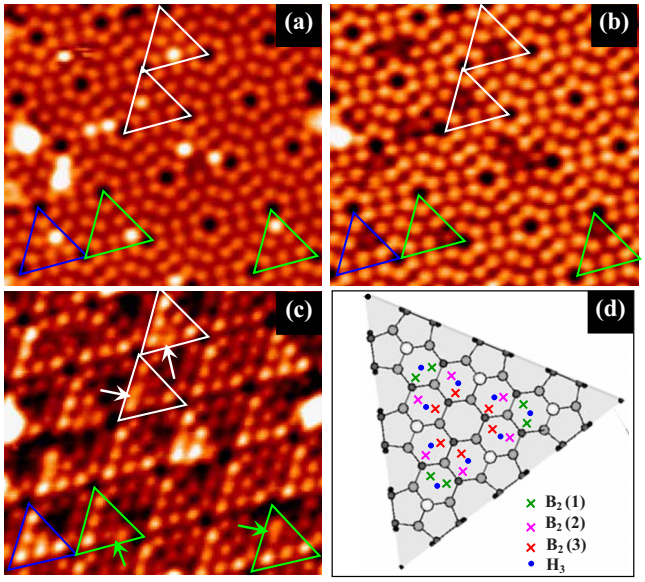

FIG. 3. (Color online) Initial adsorption stage of 0.05 ML Mn on Si(111)-7×7 deposited at 80 °C. (a) $U=+2.1$ V, 11.5 ×11.5 nm^2. (b) $U=+1.5$ V, 11.5×11.5 nm^2. (c) $U=-1.2$ V, 11.5×11.5 nm^2. The white-triangle marks correspond to the HUCs where a Mn atom adsorbed nearby the center Si adatom, the green-triangle marks correspond to the HUCs where a Mn atom adsorbed nearby the corner Si adatom, and the blue-triangle mark corresponds to the HUC where a Mn atom substituted the Si center adatom. The arrows are used to indicate the Mn adsorption sites.

"ball" shape. From the cross-section line profile shown in Fig. 2(d), we find that the center protrusion of the balls is higher than the surrounding, suggesting that this cluster has the three-dimensional nature instead of the planar structure as group-III metal clusters.[2] The pear clusters that appeared in Fig. 2(a), marked by "*P*," are off the center position of HUCs with a mirror symmetry. The orientation of mirror plane points to the directions of three Si corner holes. The sizes of the pear clusters are found to be larger than those of the identical triangle clusters. In the empty-state image of Fig. 2(b), although the morphology of pear clusters becomes irregular, the mirror symmetry still can be identified. Similarly, from the cross-section profile line in Fig. 2(d), the relative high protrusions of pear clusters indicate that it has a 3D structure.

In order to explore the cluster formation mechanism, it is necessary to study the initial adsorption stage of Mn on Si(111)-7×7. First we deposit ~0.05 ML of Mn on Si(111)-7×7 at 80 °C. The morphology of the adsorbates is presented in Fig. 3, where three sequential STM images correspond to the same sample area but at different bias. It is observed that both the aggregated Mn clusters and individual Mn adatoms coexist on the surface. The clusters seem irregular without any symmetry. The individual Mn adatoms exhibit different appearances under different bias. Similar to the case of Mn nanocluster arrays, it is observed that almost Mn adsorbates prefer to occupy the faulted HUCs.

According to the attraction-basin mechanism proposed by Cho *et al.*,[26] for most metal atoms on the Si(111)-7×7 surface, the high coordinate sites, such as B_2, T_4, and H_3, are more favorable than the T_1 sites on top of dangling bonds of adatom and rest atoms. The adsorbate atoms should be trapped into the three attraction basins and may diffuse within the basins. By careful examination and comparison of the individual Mn atom protrusions under different sample biases, we speculate that Mn atoms prefer to occupy the bridging B_2 sites around Si rest atoms and even the substitution sites of the center Si adatoms. Considering the different surrounding for the Si corner and center adatoms, the 18 B_2 sites within HUCs can be classified into three groups, referred to as $B_2(1)$, $B_2(2)$, and $B_2(3)$ as illustrated in Fig. 3(d). $B_2(1)$ is close to the corner Si adatoms, $B_2(2)$ is close to the center Si adatoms but near the HUCs edges, while $B_2(3)$ is close to Si center adatoms and the HUC's center. (i) Within each HUC, marked by white triangle, there is one Mn atom adsorbed. We noticed that the protrusion of center Si adatom becomes very bright under +2.1 V bias shown in Fig. 3(a). It becomes strongly dimmed but was still visible when the sample bias changed to +1.5 V shown in Fig. 3(b). In the filled-state image shown in Fig. 3(c), the brightness of this center Si adatoms gets normal, but its position shifted slightly toward the corner Si adatoms. Meanwhile, there is an extra protrusion that appeared at the position between Si corner adatom and the shifted Si center adatom as shown by the end point of white arrows. (ii) Within the two HUCs, marked by the green triangles, there is also one Mn atom adsorbed. It is found that the corner Si adatom becomes very bright in Fig. 3(a) and becomes strongly dimmed in Fig. 3(b). When the sample bias changed to −1.2 V in Fig. 3(c), the brightness of this Si corner adatom becomes normal, but its position is shifted slightly toward the neighboring center Si adatom. Meanwhile, an extra protrusion appeared at the position between the shifted Si corner adatom and center adatom, as shown by the end point of green arrows. Combining the above analysis, we conclude that the extra protrusions in the filled-state image correspond to the favored adsorption sites of Mn atom on Si(111)-7×7. The brightness variations of Si center or Si corner adatom in Figs. 3(a) and 3(b) can be contributed to the *charge-transfer* effect. Furthermore, we speculate that the Mn adsorption site is the bridging site around the Si rest atoms. Specifically, the Mn atom in the white HUCs occupies the $B_2(2)$ site while the Mn atom in the green HUCs occupies the $B_2(1)$ position. (iii) For the Mn atom within the blue triangle, we conclude that Mn atom has substituted the Si center adatom because there is no extra protrusion that appeared in all the three STM images. The protrusion variation of the Si center adatom is arising from Mn atom substitution of Si.

In Fig. 4 we present the topography STM images for the Mn clusters formed at the initial deposition stages. At the coverage of 0.05 ML, Mn atoms aggregated into several kinds of nanoclusters. As shown by the marks in Fig. 4(a), there are three identical clusters exhibiting unique morphology that has not been observed for the other coverages of Mn. A round protrusion appeared at HUC edges, accompanied by two-center Si adatom vacancies. It resemble the Co off-center clusters formed in the deposition of Co on Si(111)-7×7 at an elevated temperature.[27] Since both Mn and Co are transition metals here, we suppose that the structure model of identical Mn clusters is the same as that of Co

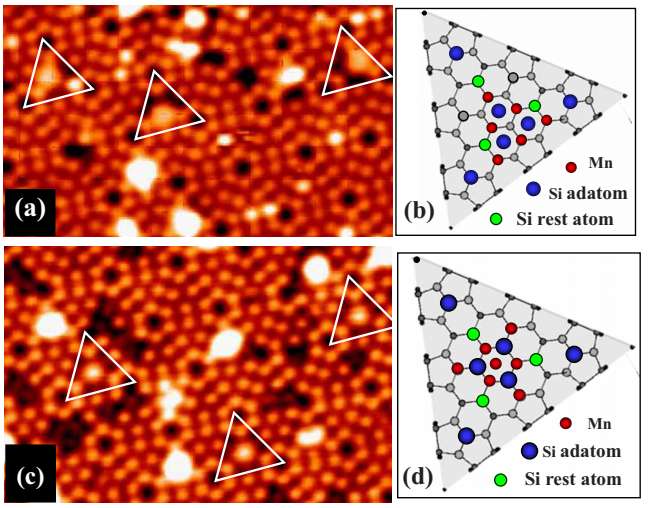

FIG. 4. (Color online) Formation of identical Mn clusters during the initial adsorption stages on Si(111)-7×7 deposited at 80 °C. (a) The identical off-center clusters formed at 0.05 ML Mn, $U=+2.0$ V, 9.5×16 nm^2. (b) Atomic structural model for the identical off-center Mn clusters with respect to Si(1110)-7×7. (c) Identical triangle clusters formed at 0.08 ML Mn, $U=+1.5$ V, 11×16 nm^2. (d) Atomic structural model for the identical triangle Mn clusters with respect to Si(111)-7×7.

clusters. Based on density functional theory calculation for Co clusters,[27] we propose a model where three librated Si adatoms, which are moved to the H_3 sites near the edge of FHUCs, are bonded with six Mn atoms. The latter occupy the six T_4 sites and have maximum numbers of bonds with Si, which is the unique character of transition metal in Si. The illustrative model for the identical off-center Mn cluster is shown in Fig. 4(b).

When the Mn coverage increased to 0.08 ML, the identical triangle clusters and pear clusters, which also appeared in the arrays of Mn nanocluster, formed in the faulted HUCs with the companies of other irregular clusters. This clearly demonstrates that the Mn clustering is a coverage-dependent process. The morphology of the two kinds of clusters in the empty-state image is shown in Fig. 4(c). Based on the 3D nature of identical triangle clusters observed at empty-state images and the bonding character of transition metal, they prefer to saturate their orbital by adsorbing at high coordination sites.[28] We proposed a structural model of Mn_7 cluster, which is shown in Fig. 4(d). First, the three Si center adatoms are substituted by Mn atoms and moved to the central three T_1 sites. Then let the three Mn atoms occupy the three T_4 site to have the maximum number of bonds on the surface. Lastly, the seventh Mn atom occupies the central H_3 site above the three Si atoms, forming a three-dimensional Mn_7 cluster. Except for the top Mn atom, the arrangement of six Mn atoms is the same as the structural model of group-III nanoclusters, such as In_6 cluster based on first-principles calculation.[2] It should be noted that both the off-center Mn clusters shown in Fig. 4(b) and the identical triangle Mn clusters in Fig. 4(d) are the proposed structural models involved in the movement of Si center adatoms to "new" position, which also occurred in the cases of In, Ga, Al nanoclsuters,[2,3] and Co reactive clusters.[27] In addition, we have also studied the effects of high deposition rates that varies from 0.05–2 ML/min, and the effect of higher substrate temperatures that varies from 100 °C to 300 °C. We found that the deposition rate of 0.01 ML combined with substrate temperature of 80 °C ~ 100 °C is the optimized parameter. Utilizing other growth parameters would reduce the preference fraction of Mn occupation of FHUCs from 95% to ~85%. This demonstrates that the formation of Mn nanocluster arrays is due to the delicate balance between thermodynamic tendency and kinetic limitation.

Regarding the microscopic mechanism of Mn nanocluster array formation, the self-organization of Mn nanoclusters can be regarded as a process of tailoring the dynamics of diffusing Mn atoms, and the preferred occupation faulted HUCs through delicate regulation of the deposition rate and substrate temperature. The optimal temperature window corresponds to the crossover between the kinetic and the thermodynamically controlled regimes. In particular, we used an extreme low-deposition rate to realize the similar effect of high-substrate temperature to avoid the possible Mn/Si reaction. As for the mechanism of coverage-dependent Mn clustering, it can be attributed to the cooperative diffusion (nonlocal attractive interactions among Mn atoms). In low coverage regime, cooperative diffusion has a negligible effect, since the spacing between Mn adsorbates is larger than the operation spatial range of interactions. Only up to a critical Mn coverage, nonlocal attractive interactions become operative and cooperative diffusion begins to influence the Mn aggregation and occupation.

IV. CONCLUSION

In conclusion, utilizing the extreme low-deposition rate, we have fabricated the highly-ordered nanoarrays of 3D Mn nanoclusters on Si(111)-7×7 surface, where the Mn nanoclusters prefer occupying the faulted HUCs of Si(111)-7×7 with preference fraction ~95%. High-resolution STM images reveal that two types of 3D Mn nanoclusters coexist on the surface; one is the identical triangle clusters and the other is the pear clusters. Studies on the initial deposition stages reveal that the individual Mn atoms prefer to reside at the bridging B_2 sites and the substitution site of Si center adatoms. It is also observed that Mn clustering is a coverage-dependent process. The identical off-center Mn cluster has been identified from the initial deposition stages. The formation mechanism of Mn nanocluster arrays is attributed to the delicate balance between thermodynamic tendency and kinetic limitation.

ACKNOWLEDGMENTS

This work was supported by the Program for New Century Excellent Talents in the University of Chinese Ministry of Education (Grant No. NCET-05-0772) and by the Natural Science Foundation of Chongqing City (Grant No. 2008BB4003).

*qkxue@tsinghua.edu.cn

[1] L. Vitali, M. G. Ramsey, and F. P. Netzer, Phys. Rev. Lett. **83**, 316 (1999).
[2] J. L. Li, J. F. Jia, X. J. Liang, X. Liu, J. Z. Wang, Q. K. Xue, Z. Q. Li, J. S. Tse, Z. Zhang, and S. B. Zhang, Phys. Rev. Lett. **88**, 066101 (2002).
[3] J. F. Jia, J. Z. Wang, X. Liu, Q. K. Xue, Z. Q. Li, Y. Kawazoe, and S. B. Zhang, Appl. Phys. Lett. **80**, 3186 (2002).
[4] O. Fruchart, M. Klaua, J. Barthel, and J. Kirschner, Phys. Rev. Lett. **83**, 2769 (1999).
[5] H. Brune, M. Giovannini, K. Bromann, and K. Kern, Nature (London) **394**, 451 (1998).
[6] M. Y. Lai and Y. L. Wang, Phys. Rev. B **64**, 241404 (2001).
[7] V. G. Kotlyar, A. V. Zotov, A. A. Saranin, T. V. Kasyanova, M. A. Cherevik, I. V. Pisarenko, and V. G. Lifshits, Phys. Rev. B **66**, 165401 (2002).
[8] P. Sobotik, O. Ostadal, J. Myslivecek, and T. Jarolimek, Surf. Sci. **454-456**, 847 (2000).
[9] I. Chizhov, G. Lee, and R. F. Willis, Phys. Rev. B **56**, 12316 (1997).
[10] Y. Hasegawa, I. Kamiya, T. Hashizume, T. Sakurai, H. Tochihara, M. Kubota, and Y. Murata, J. Vac. Sci. Technol. A **8**, 238 (1990).
[11] S. Sun, C. B. Murray, Dieter Weller, Liesl Folks, and Andreas Mose, Science **287**, 1989 (2000).
[12] K. H. Kim, J. D. Lee, J. J. Lee, S. W. Han, and J. S. Kang, J. Korean Phys. Soc. **51**, 1032 (2007).
[13] M. M. R. Evans, J. C. Glueckstein, and J. Nogami, Phys. Rev. B **53**, 4000 (1996).
[14] G. Ctistis, U. Deffke, K. Schwinge, J. J. Paggel, and P. Fumagalli, Phys. Rev. B **71**, 035431 (2005).
[15] T. Nagao, S. Ohuchi, Y. Matsuoka, and S. Hasegawa, Surf. Sci. **419**, 134 (1999).
[16] Q. Zhang, M. Tanaka, M. Takeguchi, and K. Furuya, Surf. Sci. **507-510**, 453 (2002).
[17] A. Kumar, M. Tallarida, M. Hansmann, U. Starke, and K. Horn, J. Phys. D **37**, 1083 (2004).
[18] S. M. Prokes, O. J. Glembocki, W. E. Carlos, and T. A. Kennedy, Appl. Surf. Sci. **214**, 103 (2003).
[19] S. Azatyan, M. Hirai, M. Kusaka, and M. Iwami, Appl. Surf. Sci. **237**, 105 (2004).
[20] S. G. Azatyan, M. Iwami, and V. G. Lifshits, Surf. Sci. **589**, 106 (2005).
[21] D. Y. Wang, H. Y. Wu, L. J. Chen, W. He, Q. F. Zhan, and Z. H. Cheng, J. Phys.: Condens. Matter **18**, 6357 (2006).
[22] D. Y. Wang, L. J. Chen, W. He, Q. F. Zhan, and Z. H. Cheng, J. Phys. D **39**, 347 (2006).
[23] H. Wang and Z. Q. Zou, Appl. Phys. Lett. **88**, 103115 (2006).
[24] E. Vasco, Surf. Sci. **575**, 247 (2005); E. Vasco, Phys. Rev. B **69**, 075412 (2004).
[25] K. H. Wu, Y. Fujikawa, T. Nagao, Y. Hasegawa, K. S. Nakayama, Q. K. Xue, E. G. Wang, T. Briere, V. Kumar, Y. Kawazoe, S. B. Zhang, and T. Sakurai, Phys. Rev. Lett. **91**, 126101 (2003).
[26] K. Cho and E. Kaxiras, Surf. Sci. **396**, L261 (1998).
[27] M. A. K. Zilani, Y. Y. Sun, H. Xu, Lei Liu, Y. P. Feng, X. S. Wang, and A. T. S. Wee, Phys. Rev. B **72**, 193402 (2005).
[28] P. A. Bennett, D. G. Cahil, and M. Copel, Phys. Rev. Lett. **73**, 452 (1994).